CLIMATOLOGY

Increased U.S. coastal hurricane risk under climate change

Karthik Balaguru[1]*, Wenwei Xu[1], Chuan-Chieh Chang[1], L. Ruby Leung[1], David R. Judi[1], Samson M. Hagos[1], Michael F. Wehner[2], James P. Kossin[3], Mingfang Ting[4]

Copyright © 2023 The Authors, some rights reserved; exclusive licensee American Association for the Advancement of Science. No claim to original U.S. Government Works. Distributed under a Creative Commons Attribution NonCommercial License 4.0 (CC BY-NC).

Several pathways for how climate change may influence the U.S. coastal hurricane risk have been proposed, but the physical mechanisms and possible connections between various pathways remain unclear. Here, future projections of hurricane activity (1980–2100), downscaled from multiple climate models using a synthetic hurricane model, show an enhanced hurricane frequency for the Gulf and lower East coast regions. The increase in coastal hurricane frequency is driven primarily by changes in steering flow, which can be attributed to the development of an upper-level cyclonic circulation over the western Atlantic. The latter is part of the baroclinic stationary Rossby waves forced mainly by increased diabatic heating in the eastern tropical Pacific, a robust signal across the multimodel ensemble. Last, these heating changes also play a key role in decreasing wind shear near the U.S. coast, further aggravating coastal hurricane risk enhanced by the physically connected steering flow changes.

INTRODUCTION

Hurricanes rank among the leading causes of economic damages in the United States annually (*1*–*3*) with wide-ranging societal impacts upon landfall (*4*, *5*). It is thus of great socioeconomic and scientific interest to understand how the risk associated with hurricanes will evolve in the future climate. As the planet continues to warm, global hurricane risk is expected to rise (*1*, *6*–*11*), because of increases in storm maximum intensity (*11*–*15*), decreases in translation speed (*11*, *16*–*18*), increasing near-center precipitation rate (*19*–*21*), and shifting tracks (*22*). However, examining changes in storm characteristics at global or basin scales can occasionally mask notable regional shifts in climate model simulations, making it difficult to interpret hurricane risk locally. Therefore, besides exploring changes in various aspects of hurricanes on the global scale, a better understanding of how hurricane characteristics will evolve on regional scales is particularly important for assessing future losses resulting from landfalling storms. As indicated by a number of studies, anticipated stalling of storms (*16*–*18*, *23*), increasing hurricane intensification rates (*24*, *25*), and slower dissipation after landfall (*26*) could pose greater hazards to coastal communities in future (*27*). In addition, future growth in population and wealth along the U.S. Gulf and East coasts combined with rising sea levels (*6*, *15*) could further exacerbate the risk associated with landfalling hurricanes (*2*).

Despite this, the physical mechanisms responsible for how anthropogenic climate change will influence certain aspects of hurricanes in the nearshore region are not well understood. For instance, climate models project a robust decrease in vertical wind shear near the U.S. coast (*24*, *25*, *28*, *29*), but the underlying physical rationales have not been firmly established. Similarly, the relative importance of various processes leading to the slowdown of storms (*16*–*18*, *23*) and changes in hurricane landfall (*30*–*34*) remains unclear. Beyond physical understanding, robust quantification of anthropogenic influence on near-coastal hurricane characteristics is difficult to achieve on the basis of observations and dynamical models (*15*, *35*). On average, only one to two hurricanes make landfall each year over the continental United States (*2*), and such limited historical records are not enough to derive meaningful estimates of how the long-term risk posed by the hurricanes may respond to a changing climate (*35*, *36*). General circulation models (GCMs) are the most straightforward approach to assessing the impact of climate change on hurricane risk as they directly simulate hurricane evolution based on physical laws. However, it is computationally expensive to generate a sufficient number of storms for hazard assessment because high spatial resolutions are necessary to realistically simulate the distributions of storm tracks and intensities (*15*, *37*, *38*).

Consequently, statistical-dynamical downscaling methods exploiting the dependence of hurricane climatology on the large-scale storm environment have been developed to generate large ensembles of synthetic hurricane tracks (*35*, *36*, *39*). In this study, we use the Risk Analysis Framework for Tropical Cyclones (RAFT) (*40*), a hybrid modeling approach that combines physics, statistics, and machine learning to produce a large number of synthetic hurricanes, including tracks and along-track intensities (see Materials and Methods and text S1), to understand how the U.S. coastal hurricane risk may change with projected climate change. Subsequently, we use a nonlinear stationary wave model (SWM) (*41*) to uncover the dynamical mechanisms that play a key role in the evolving coastal hurricane risk.

RESULTS

The coastal hurricane frequency (CHF) (*42*), estimated on the basis of RAFT (*40*) and environmental fields from National Centers for Environmental Prediction (NCEP) (*43*) and ECMWF Reanalysis v5 (ERA5) (*44*) (see Materials and Methods), is shown in Fig. 1A over the historical period of 1979–2018. The CHF is defined as the number of 6-hour overland hurricane track locations per square degree per year, where the storm intensity exceeds a threshold

[1]Pacific Northwest National Laboratory, Richland, WA, USA. [2]Lawrence Berkeley National Laboratory, Berkeley, CA, USA. [3]The Climate Service, an S&P Global Company, Madison, WI, USA. [4]Lamont-Doherty Earth Observatory, Columbia University, Palisades, NY, USA.
*Corresponding author. Email: karthik.balaguru@pnnl.gov

Downloaded from https://www.science.org on June 18, 2024

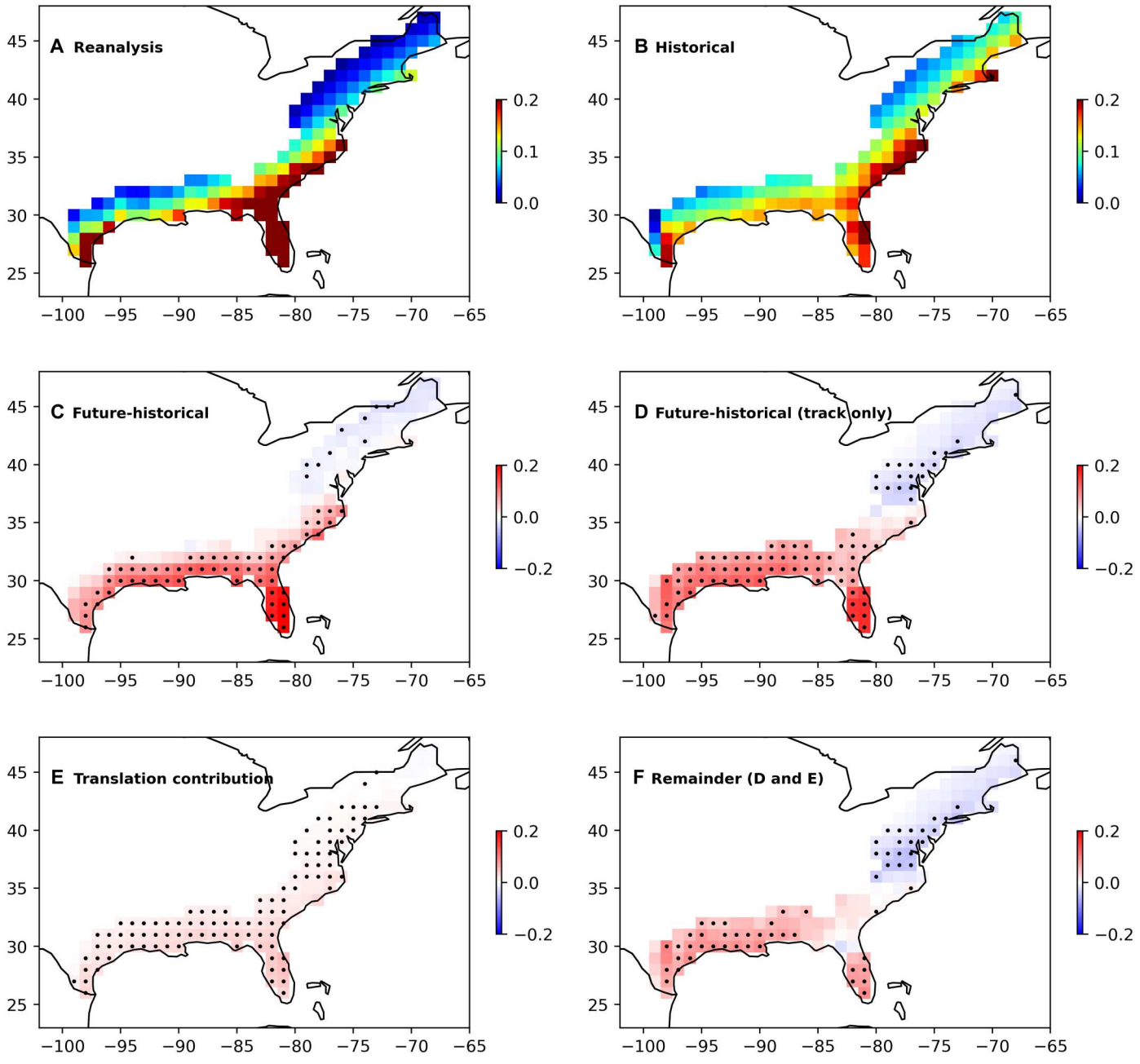

Fig. 1. Projected change in U.S. hurricane risk based on Risk Analysis Framework for Tropical Cyclones (RAFT). (**A**) Climatological coastal hurricane frequency (CHF), defined as the number of 6-hour hurricane track locations per square degree per year, obtained when RAFT is used with reanalysis (1979–2018). All track locations where the storm intensity exceeds 25 knots are used. (**B**) Climatological CHF obtained when RAFT is used with historical phase 6 of the Coupled Model Intercomparison Project (CMIP6) simulations. Ensemble mean of eight models for the historical period 1980–2014 is shown. All track locations where the storm intensity exceeds 21.5 knots are used to estimate CHF. (**C**) Change in CHF for the future period (2066–2100) with respect to the historical period (1980–2014) under the SSP585 emissions scenario. (**D**) As in (C) but based only on the track model in RAFT. A 2-day cutoff is used to truncate tracks over land. (**E**) Change in CHF for the future period based on projected change in translation speed. (**F**) Contribution of projected change in landfall to future change in CHF estimated as the difference between (D) and (E). In (C) to (F), black dots indicate those locations where seven of the eight models agree on the sign of the change.

Downloaded from https://www.science.org on June 18, 2024

(see Materials and Methods). The potential threat that hurricanes pose to coastal communities can be assessed using the CHF because it considers the combined effects of hurricane frequency, intensity, track patterns, and translation speeds. As revealed in Fig. 1A, the Gulf Coast and the lower East Coast (south of 40°N) have experienced higher hurricane risk than the upper East Coast (north of 40°N) from 1979 to 2018. Regions that have been particularly vulnerable to hurricanes include the lower East Coast, Florida, and the coasts of Texas and Louisiana (Fig. 1A). Furthermore, CHF simulated with the reanalysis datasets is in reasonable agreement with that obtained using the best-track data (fig. S1A) with a pattern correlation of about 0.7 (significant at the 99% confidence level) and a mean absolute error of about 0.05, demonstrating the ability of RAFT to quantitatively estimate the risk posed by hurricanes for the coastal regions. Next, environmental fields derived from eight climate models belonging to phase 6 of the Coupled Model Intercomparison Project (CMIP6) (*45*) are used with RAFT (see Materials and Methods). The spatial pattern of CHF obtained by applying RAFT to the historical CMIP6 simulations, covering the period 1980–2014, shows broad agreement with that generated using reanalysis (a pattern correlation of 0.85 that is significant at the 99% level and a mean absolute error of about 0.04) as it presents higher CHF along the lower East Coast, over Florida peninsula and near the Texas coast (Fig. 1B). However, some biases in the magnitude are visible. RAFT forced with the environmental fields from CMIP6 simulations tends to underestimate the CHF over Florida peninsula, and the CHF near the upper East Coast is somewhat overestimated during 1980–2014. Despite the discrepancies, many aspects of the observed CHF (fig. S1A) are captured by RAFT during the historical period when combined with the CMIP6 multimodel ensemble.

Now, we consider potential changes in CHF under "SSP585," a future climate scenario in which the planet's radiative forcing is expected to increase by about 8.5 Wm^{-2} at the end of the 21st century (*46*). Changes in CHF for the future period (2066–2100) with respect to the historical period (1980–2014) are positive over much of the Gulf Coast and the lower East Coast (Fig. 1C), with the largest increases projected to occur over the northern Gulf Coast and Florida peninsula. However, for the upper East Coast, the CHF anomalies are weakly negative and largely insignificant. Because changes in the CHF include the joint effects of intensity and steering flow, we next examine the changes in CHF based only on the track model within RAFT to isolate the role of steering flow. The results based on the track model, assuming no change in hurricane intensity (Fig. 1D), suggest that the CHF will likely increase over much of the Gulf Coast, Florida peninsula, and the lower East Coast and decrease near the upper East Coast and are largely consistent with those based on the combined changes of intensity and tracks (Fig. 1C). The similarity between Fig. 1C and Fig. 1D indicates that differences in steering flow are the major drivers for the overall change in CHF. Further decomposing the effects of steering flow (see Materials and Methods) reveals that the contribution from translation speed (Fig. 1E) is notable but weakly positive for most coastal areas. The positive contribution of translation speed to CHF is due to a slowing down or stalling of storms over the US (Fig 2B), which is projected to occur under climate change by some studies (*16*–*18*). Besides translation speed, landfall or a shift in tracks is the other important pathway through which the steering flow affects CHF. Note that the spatiotemporal distribution of genesis is held fixed for both the historical and future periods, in part due to the ambiguity associated with future projections of Atlantic hurricane genesis (see text S1 for further details). Nevertheless, an examination of CHF changes projected by high-resolution climate models points toward potential regional uncertainty associated with results based on RAFT that ignores genesis changes, especially for the lower East Coast (see text S2). Despite the limitations associated with the representation of genesis in RAFT, the framework provides an effective means to isolate the role of steering flow in the evolving hurricane risk. The impact of changes in hurricane track pattern on CHF, obtained as the difference between Fig. 1D and Fig. 1E (see Materials and Methods), suggests that it plays the dominant role. More specifically, the dipole-like spatial pattern of a broad increase in CHF over the Gulf and lower East Coast regions, and a projected decrease in CHF near the upper East Coast, can mainly be attributed to steering flow-induced changes in hurricane tracks. The map of changes in hurricane strike probabilities along the coast (fig. S2) is consistent with this assessment.

Because future changes in CHF projected by RAFT are mainly caused by shifts in tracks, we now explore how the environmental steering flow and its associated large-scale winds will evolve as climate changes. Changes in the multimodel ensemble mean steering flow (Fig. 2A) under the SSP585 scenario reveal that the steering flow is projected to become more easterly near the East Coast and more southeasterly in the Gulf of Mexico. Away from the East Coast, the steering flow will become northeasterly over much of the North Atlantic, especially north of 20°N. At the basin scale, the change in hurricane frequency projected by RAFT (fig. S1D) suggests a large increase over the western Atlantic and a weak decrease over the eastern Atlantic. The increase over the western Atlantic occurs because of two reasons. First, the change in hurricane steering flow shifts tracks westward and closer to the U.S. coast. Second, the westward shift in tracks causes storms to go through a climatologically more favorable environment in the western part of the basin. Consequently, there is a substantial enhancement of hurricane frequency over the western Atlantic that leads to an increase in CHF for the Gulf Coast and lower East Coast regions (Fig. 1C).

Also, these changes in steering flow tend to oppose the climatological steering flow pattern and will decrease the hurricane translation speed in the subtropical North Atlantic and over the continental United States (Fig. 2B). This is consistent with the influence of translation speed on CHF noted earlier (Fig. 1E). In RAFT, the steering flow is defined as a weighted mean of winds at 200 and 850 hPa. Examining changes of winds at different levels separately shows that steering flow changes are dominated by the 200-hPa anomalous easterlies and southeasterlies close to the U.S. coast (Fig. 2C) and by those at 850 hPa away from the U.S. coast in the North Atlantic (Fig. 2D). At 200 hPa, the development of a cyclonic circulation anomaly above the Gulf of Mexico (Fig. 2C) is visible, and the northern branch of the cyclone decelerates the westerlies north of 30°N and may cause a considerable slowdown of storms near the populated coastal regions (*18*, *16*). Changes in 850-hPa winds are northeasterly north of 30°N, and northerly between 20°N and 30°N (Fig. 2D). In addition, the intensifying easterly trades over the Caribbean sea tend to accelerate storm motion over this area, consistent with previous studies (*18*). While these results are based on winds at the 200- and 850-hPa levels, additional

Downloaded from https://www.science.org on June 18, 2024

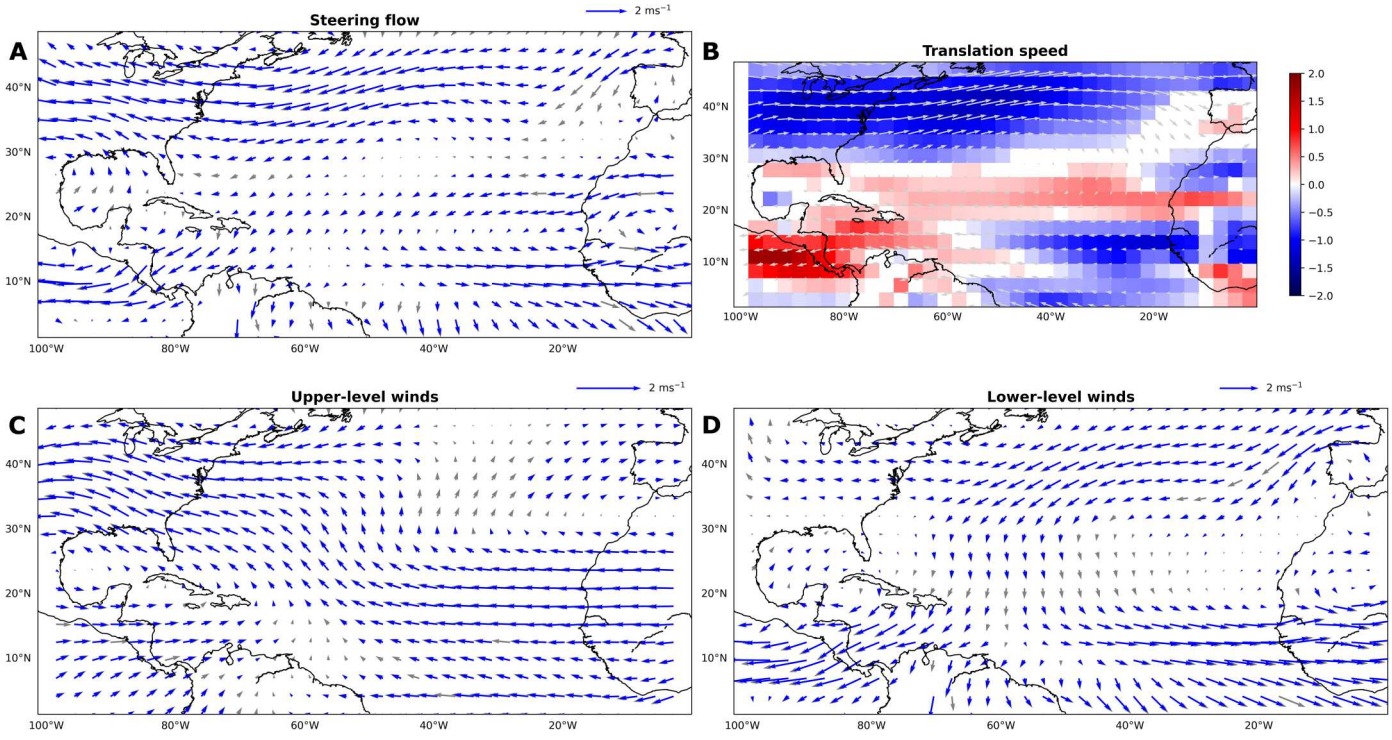

Fig. 2. Projected changes in the environmental steering flow under the SSP585 scenario. (**A**) Vector changes in steering flow. (**B**) Changes in translation speed (shaded) with vectors of climatological steering flow from the historical period overlaid. Vector changes in winds at (**C**) upper level (200 hPa) and (**D**) lower level (850 hPa). Note that the winds at the upper and lower levels are multiplied by 0.2 and 0.8, respectively, to reflect their relevance to the steering flow. Changes are based on the ensemble mean of eight phase 6 of the Coupled Model Intercomparison Project (CMIP6) models. All parameters are averaged over the months of August to October. "Change" indicates the difference between the mean over the future period (2066–2100) and the historical period (1980–2014). In (A), (C), and (D), blue arrows indicate locations where changes in vector magnitude are statistically significant at the 95% level based on the Student's *t* test. In (B), nonwhite shaded areas represent locations where changes in translation speed are significant at the 95% level based on the Student's *t* test.

analysis indicates that they are not sensitive to the exact definition of steering flow used (fig. S3).

Diagnoses using RAFT delineate the dominant role of steering flow in driving the heightened U.S. coastal hurricane risk under a changing climate and motivate us to explore the following important question: What are the underlying dynamical mechanisms responsible for changes in the large-scale hurricane steering flow? Climatological steering flow is principally shaped by geographically fixed low-frequency circulation patterns, such as the subtropical high (*47*), which are an integral part of the stationary waves. These planetary-scale, zonally asymmetric circulation features are relatively stable on the seasonal time scales and arise because of longitudinal asymmetries in topography, diabatic heating, and synoptic eddies (*48*, *49*, *50*). Also, they are influenced by the structure of the background zonal-mean flow (*51*). Here, to better understand the key physical driver in the CMIP6 models, we carry out seven idealized sensitivity experiments with the SWM (table S1). The control run (CTRL) computes deviations from a prescribed zonally symmetric mean state in response to the diabatic heating, transient eddies, and topography in the present (1980–2014) climate. Simulations for the future period (2066–2100) are conducted by applying the basic state and various asymmetric forcings projected by CMIP6 models under the SSP585 emissions scenario as perturbations to the CTRL. The relative contribution of the anomalous basic state, diabatic heating, and transient forcing to the projected total change in circulation is assessed by the following sensitivity runs: CTRL + ΔBS, CTRL + ΔDH, and CTRL + ΔTranF, respectively. In each experiment, only the future input of interest is used and all other inputs are fixed at their historical values. See text S3 for a more detailed description of the model and its validation.

As revealed by the ensemble mean of CMIP6 projections, the tropospheric response to the increasing anthropogenic forcing is characterized by a vertical phase reversal between 10°N and 40°N (Fig. 3, A and B). At 850 hPa, a region of positive streamfunction (ψ) anomaly with anticyclonic flow extends from the Caribbean Sea in the Atlantic to about 120°W in the eastern Pacific, and two anomalous lows are located over the subtropical central Pacific and the eastern North Atlantic (Fig. 3A). The projected lower tropospheric circulation pattern suggests a potential westward shift or expansion of the North Atlantic subtropical high (*52*), which has been regarded to have important implications for the U.S. regional precipitation in a warmer climate (*53*). Meanwhile, the strengthened upper-level cyclonic circulation above the far-eastern North Pacific and the Gulf of Mexico plays a decisive role in steering flow changes near the U.S. coast, as noted earlier (Fig. 2A). When the SWM is subject to simultaneous changes in basic states, diabatic heating, and transient eddies, the spatial pattern of the coupled model's circulation response is qualitatively reproduced at both 850- and 200-hPa levels (Fig. 3, C and D). The magnitude of ψ difference, however, is somewhat overestimated in the model, particularly for the anomalous

Downloaded from https://www.science.org on June 18, 2024

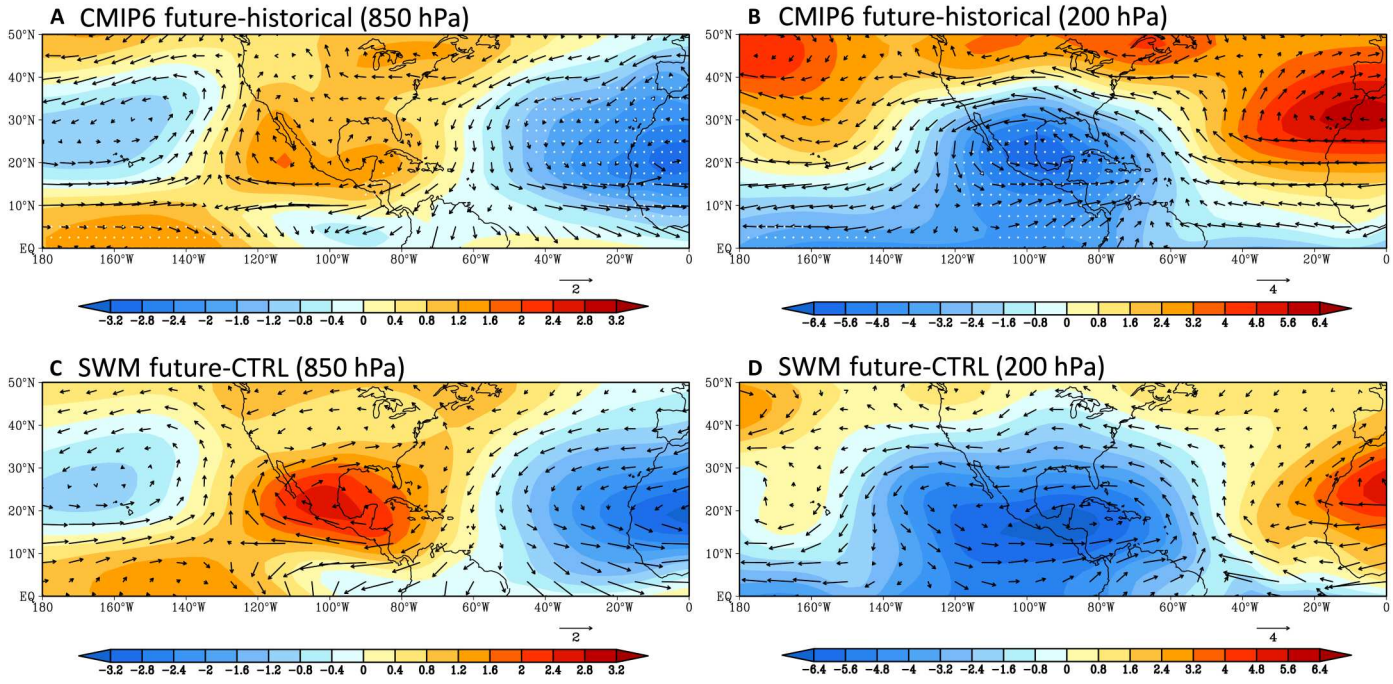

Fig. 3. Changes in the large-scale wind patterns under the SSP585 scenario simulated by the stationary wave model (SWM). Projected changes in streamfunction (shaded, 10^6 m^2s^{-1}) and winds (vector, ms^{-1}) simulated by the ensemble mean of eight phase 6 of the Coupled Model Intercomparison Project (CMIP6) models at (**A**) 850 and (**B**) 200 hPa. In (A) and (B), white stippling denotes the areas where the changes in streamfunction are statistically significant at 95% level based on the Student's *t* test. (**C**) and (**D**) are same as (A) and (B), but for changes simulated by the SWM. All parameters are averaged over the months of August to October. Change indicates the difference between the mean over the future period (2066–2100) and the historical period (1980–2014). EQ, equator.

high centered over the Central American region at 850 hPa (Fig. 3C).

Because the SWM reasonably reproduces the large-scale dynamical response of CMIP6 models to anthropogenic forcing, it allows us to further examine the effect of each forcing mechanism and understand their relative importance. In particular, the primary goal is to understand the physical drivers behind the anomalous 200-hPa cyclonic circulation (Fig. 3B). The changing zonal-mean basic state partially contributes to the increased landfall probability (Fig. 1, D and F) possibly through the enhanced easterlies over the subtropical northwestern Atlantic and the coastal regions of the Gulf of Mexico (Fig. 4A). The weakening of westerly wind occurs over a broad latitude band between 0° and 30°N (Fig. 4A) and is consistent with the poleward shift of the zonal-mean midlatitude jet in the Northern Hemisphere (fig. S4A), which has been robustly projected by various climate models (*18*, *54*, *55*). According to the thermal-wind relationship, such jet response requires a broad warming expansion from the tropics to about 40°N (fig. S4A), and the adiabatic warming in the subtropical mid- and upper troposphere can be further traced back to the enhanced descending motion driven by transient eddies (*54*). On the other hand, the response to the anomalous transient momentum forcing is relatively weak in the SWM (fig. S4B), and both changes in the zonal-mean basic state and transient forcing are unable to explain the enhanced 200-hPa cyclonic winds in a warmer climate (Fig. 3B).

The strengthening of upper tropospheric cyclonic circulation with global warming is primarily caused by changes in diabatic heating (Fig. 4B). Underneath the broad cyclonic circulation, a low-level anticyclonic anomaly forms over the Central American region, which extends over large swaths of the southern United States and into the Atlantic storm-track region. Also, it is worth noting that the easterly trades in the lower troposphere (Fig. 4C), as well as the upper tropospheric westerly winds, intensify (Fig. 4B) in response to variations of tropical heating (Fig. 4D) over the Caribbean Sea. Such flow differences help to explain why several studies (*25*, *28*, *56*) found a secular increase of vertical wind shear over this region in different climate model projections. Furthermore, the baroclinic circulation response (Fig. 4, B and C) excited by the diabatic cooling in the tropical North Atlantic and the positive heating anomalies over the tropical northeastern Pacific (Fig. 4D) is largely consistent with the Gill model's solution (*57*). Previously, it has been proposed that the formation of such a heat-induced stationary baroclinic Rossby wave is mainly reinforced by the anomalous diabatic cooling over the tropical North Atlantic in the late 21st century (*56*). To test this hypothesis, two sensitivity experiments (i.e., CTRL + ΔPacDH and CTRL + ΔAtlDH in table S1) are further carried out. However, our results draw a different conclusion and suggest that the positive heating anomalies over the tropical Pacific sector (fig. S5A) play a dominant role in maintaining the anomalously extensive baroclinic circulation extending from eastern Africa to the northeastern Pacific (fig. S5, B and C), with the secondary contribution coming from the anomalous diabatic cooling over the tropical North Atlantic (fig. S5, D to F). A weaker baroclinic atmospheric response (fig. S5, E and F) is found when the SWM is forced by regional diabatic cooling shown in fig. S5D.

So far, we have seen how future changes in the large-scale winds forced by heating changes in the tropics can affect U.S. hurricanes

Downloaded from https://www.science.org on June 18, 2024

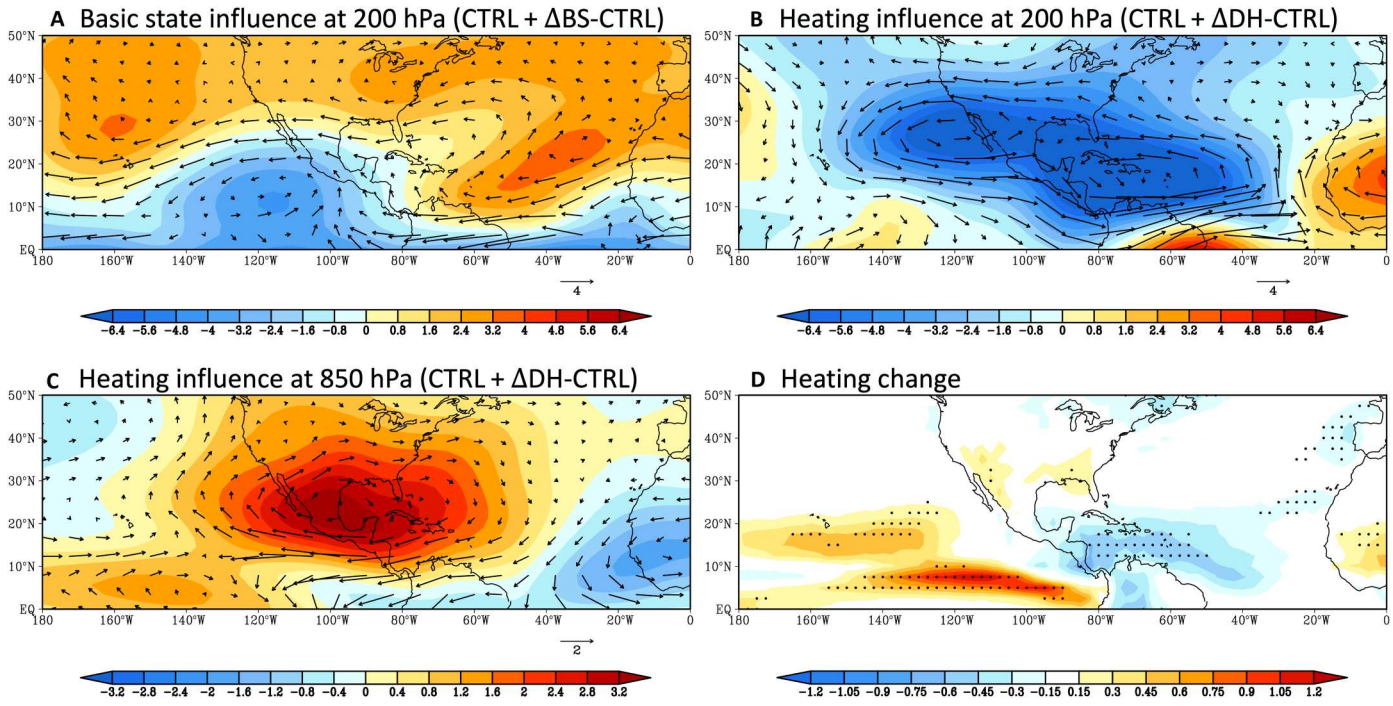

Fig. 4. Understanding changes in the large-scale wind patterns under the SSP585 scenario using the stationary wave model (SWM). (**A**) Contribution from the anomalous zonal-mean basic state to changes in the streamfunction (shaded, 10^6 m^2s^{-1}) and winds (vector, ms^{-1}) at 200 hPa. (**B**) Same as (A), but for the contribution from the anomalous zonally asymmetric diabatic heating. (**C**) Same as (B), but at 850 hPa. (**D**) Projected changes in column-averaged pressure-weighted diabatic heating ($K\ day^{-1}$). Stippling indicates locations where the ensemble-mean changes are statistically significant at the 95% level. All parameters are averaged over the months of August to October. Change indicates the difference between the mean over the future period (2066–2100) and the historical period (1980–2014). EQ, equator.

and landfall through their influence on steering flow. However, the projected changes of winds at different levels can also affect the vertical wind shear near the U.S. coast. The CMIP6 multimodel ensemble suggests that wind shear will likely reduce near the East Coast of the United States and the northern Gulf of Mexico (Fig. 5A), in line with several previous studies (*24*, *25*, *28*, *29*). When the SWM is forced by simultaneous changes in basic states, diabatic heating, and transient eddies, it broadly reproduces the spatial pattern of wind shear responses over the North Atlantic and the eastern Pacific (Fig. 5B). In particular, the SWM consistently shows a decrease in shear near the East and Gulf coastal regions (Fig. 5B). Further analysis reveals that changes in diabatic heating are primarily responsible for the shear reduction near the coast (Fig. 5C) with the secondary contribution coming from the changing basic state (Fig. 5D). Thus, in addition to altering the steering flow, future changes in diabatic heating could lead to increases in hurricane intensification (*24*, *25*) and tropical cyclogenesis (*34*) near the U.S. coast through the influence on wind shear, highlighting the broad implication of the mechanism identified in this study. Nevertheless, the projected decrease in translation speeds over the subtropical North Atlantic (Fig. 2B) is mainly driven by changes in basic state (fig. S6), which can be likely linked to the poleward shift of the midlatitude westerlies (*18*).

DISCUSSION

Several studies examined shifts in hurricane tracks, at global and regional scales, in observations and future climate projections (*18*, *22*, *30*–*34*). However, considerable uncertainty remains regarding the effect of steering flow changes with some studies favoring an increase in U.S. hurricane landfall (*34*) and others projecting a predominant decrease (*31*, *33*). A physical rationale for the projected changes in steering flow has not been established. In this study, we address this using a suite of numerical simulations based on RAFT and a SWM. With a large number of synthetic tracks simulated by RAFT which overcome the GCM hurricane sampling issue, our results indicate that future changes in steering flow will likely favor an increase in CHF, especially for the Gulf Coast and lower East Coast. Furthermore, changes in the steering flow are mainly driven by the projected strengthening of an upper tropospheric cyclonic circulation above the Gulf of Mexico, which can be regarded as a Gill-type response to the enhanced heating in the eastern tropical Pacific and diabatic cooling over the tropical North Atlantic (Fig. 6). Although simulations based on RAFT project an average increase in CHF of 37 ± 30% for the U.S. Gulf and Atlantic coasts, it must be noted that the use of a time-invariant genesis may introduce some uncertainties in these estimates. A qualitative examination of results based on high-resolution climate models suggests that changes in cyclogenesis may overwhelm the effects of steering flow changes in certain regions (text S2). Therefore, studies that address the ambiguity associated with a shift in genesis are needed to further reduce the uncertainty in our projections of future hurricane risk.

In this study, we have also demonstrated the sensitivity of projected large-scale winds to tropical heating, or precipitation changes, which are largely governed by the spatial pattern of

Downloaded from https://www.science.org on June 18, 2024

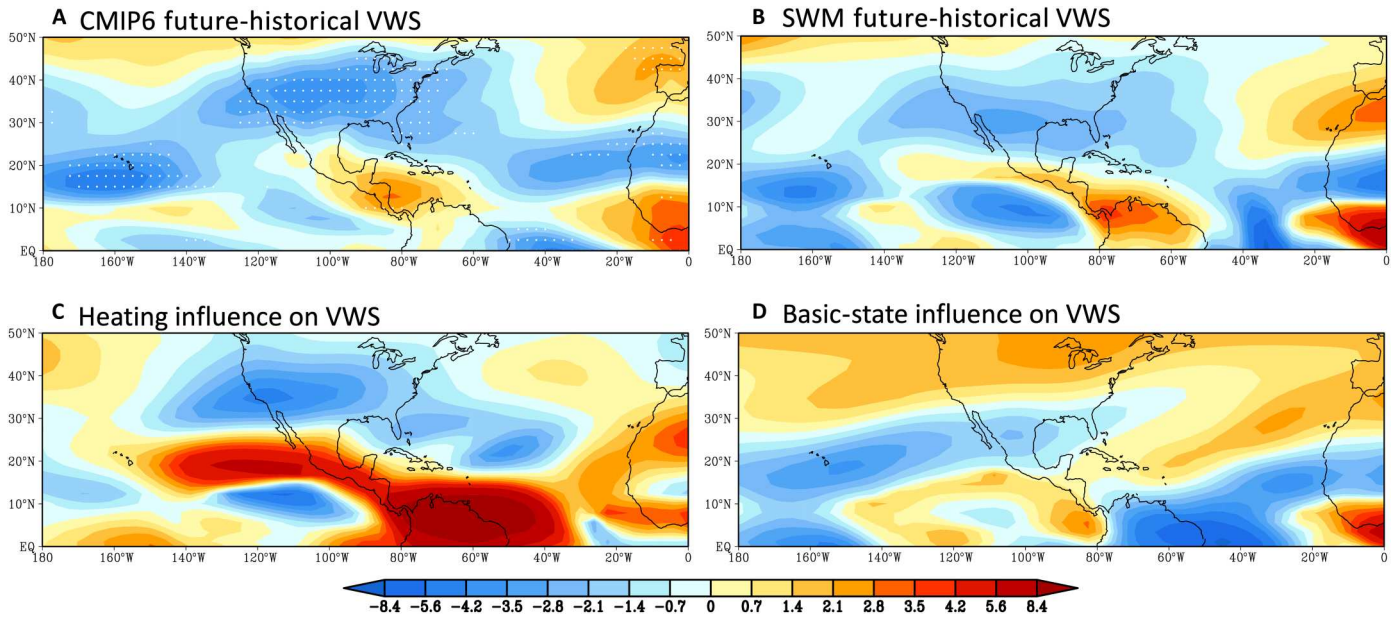

Fig. 5. Understanding changes in vertical wind shear under the SSP585 scenario. (**A**) Projected changes in wind shear (ms^{-1}) by the ensemble mean of eight phase 6 of the Coupled Model Intercomparison Project (CMIP6) models. White stippling denotes the regions where the changes in wind shear are statistically significant at the 95% level. VWS, vertical wind shear. (**B**) is same as (A), but for changes simulated by the SWM. (**C**) Contribution from the anomalous diabatic heating to changes in shear. (**D**) Same as (C), but for contribution from the anomalous zonal-mean basic state. EQ, equator.

future sea surface temperature (SST) warming (*58*–*60*). The physical framework of relative SST warming is mainly built upon thermodynamic considerations. In the tropics, upper tropospheric warming is nearly uniform and approximately follows tropical-mean SST warming (*58*) because temperature gradients are quickly adjusted by equatorial waves (*61*, *62*). In contrast, the moist static energy in the boundary layer is strongly modulated by the local SST (*63*). Enhanced local SST warming therefore leads to a regional destabilization of the atmosphere and favors the occurrence of convective precipitation, enhancing diabatic heating. Correlation analysis indicates that the intermodel uncertainty of projected heating trends over the tropical Pacific and the Maritime continent is strongly constrained by the response of the equatorial Pacific zonal SST gradient to climate change (fig. S7B), suggesting the need to reduce the differences in SST projection (fig. S7A). Some studies suggested a shift toward a more El Niño–like mean state under global warming (*58*). While CMIP5 models show large uncertainty in such SST warming patterns, a strong consensus has emerged in the CMIP6 multimodel ensemble regarding the El Niño–like warming pattern under climate change (*64*), but the differences between the CMIP5 and CMIP6 SST warming patterns are not well understood. Important sources contributing to the uncertainty of future SST warming pattern include large-scale ocean dynamics (*65*, *66*), cloud-radiation feedback (*67*), wind-evaporation SST feedback (*68*), and internal variability associated with the Interdecadal Pacific Oscillation (*64*). A better representation of these physical processes in the climate models and improved observations that can be used to further constrain the parameterized model physics are expected to increase our confidence in future projections of large-scale circulation (*68*). Last, large ensemble simulations also help to better quantify the projected uncertainty associated with internal climate variability.

MATERIALS AND METHODS

Data

Hurricane track data are obtained from the National Hurricane Center's HURDAT2 database and used to compute the CHF. Data for the large-scale hurricane environment are obtained from NCEP reanalysis (*43*) and ERA5 reanalysis (*44*) and used with RAFT to produce synthetic hurricane tracks for the historical period (*40*). First, monthly mean winds at a spatial resolution of 2.5° from NCEP reanalysis are used to generate hurricane steering flow and vertical wind shear. Next, to generate intensity along tracks, potential intensity and other thermodynamic parameters that play a key role in hurricane intensification are estimated on the basis of ERA5 reanalysis, which has a spatial resolution of about 0.3°. This is, in part, due to the smaller spatial scales of thermodynamic parameters like SST and relative humidity compared to dynamical wind fields. The results show that RAFT can well represent the salient features of Atlantic hurricanes, including the spatial distribution of tracks and lifetime maximum intensities (*40*).

Similarly, data for the large-scale environment are obtained from eight fully coupled climate models belonging to CMIP6 (*45*): Canadian Earth System Model (CanESM5), Euro-Mediterranean Centre on Climate Change–coupled climate model (CMCC-CM2-SR5), EC-Earth Consortium Model (EC-Earth3), Geophysical Fluid Dynamics Laboratory Climate Model (GFDLCM4), Institute Pierre Simon Laplace Climate Model (IPSL-CM6A-LR), Model for Interdisciplinary Research on Climate (MIROC6), Max Planck Institute Earth System Model (MPI-ESM1-2-LR), and Meteorological Research Institute Earth System Model (MRI-ESM2-0). The choice of these eight models is based on the availability of data for both the "historical" period and the "future" period under the SSP585 emissions scenario (*46*). A sensitivity analysis has been conducted by computing trends in steering flow and diabatic heating using the

Downloaded from https://www.science.org on June 18, 2024

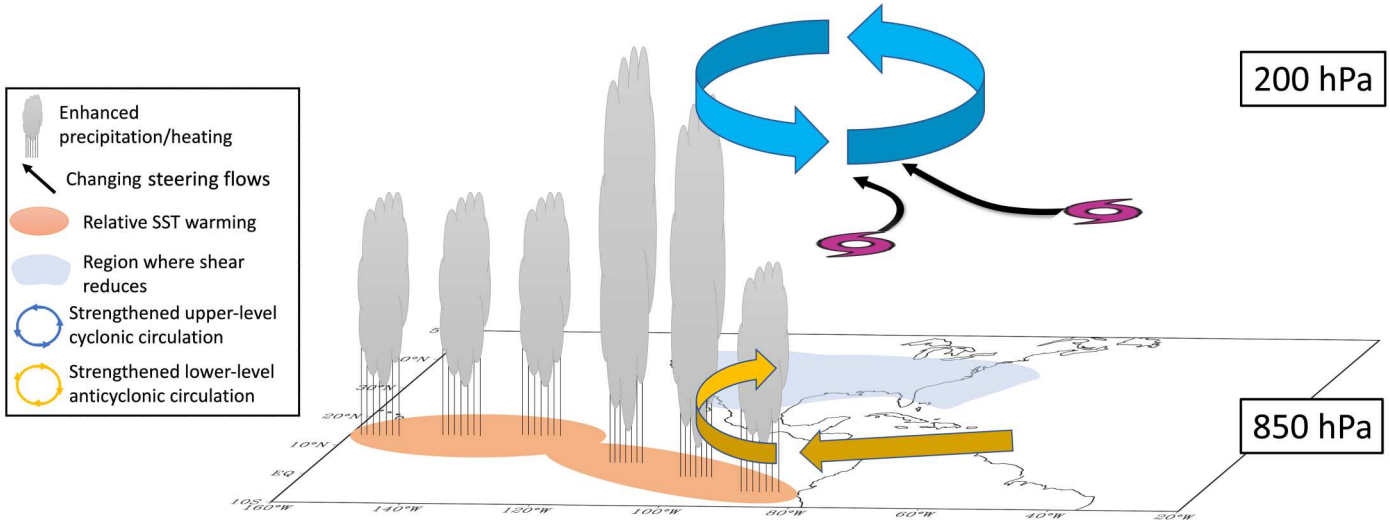

Fig. 6. Schematic illustration of the main mechanisms of coastal hurricane frequency (CHF) changes identified in this study. As the climate warms, an increase in CHF for the U.S. Gulf and lower East coasts is projected to occur and is driven primarily by changes in steering flow. The strengthening upper tropospheric cyclonic circulation above the western Atlantic plays a pivotal role in the steering flow changes. Also, the contrasting upper- and lower-level circulation anomalies reduce the vertical wind shear near the U.S. coastal regions. These changes in circulation can be regarded as a response to the projected increases in diabatic heating and warmer sea surface temperature (SST) over the eastern tropical Pacific, which is a robust signal across the phase 6 of the Coupled Model Intercomparison Project (CMIP6) multimodel ensemble.

SSP585 simulations only and by considering more than 40 CMIP6 models. The results obtained suggest that these eight models are broadly representative of the CMIP6 multimodel ensemble. Last, hurricane tracks from a suite of high-resolution climate model simulations (*69*) belonging to High Resolution Model Intercomparison Project (HighResMIP) (*70*) are used to generate projections of CHF and compare with RAFT (text S2).

Synthetic hurricane model

The RAFT (*40*) is a hybrid modeling approach that can generate large ensembles of hurricanes with realistic spatial track patterns and distributions of intensity. Genesis locations are randomly sampled from a Gaussian spatiotemporal probability distribution based on historical observations (*35*). Tracks are then generated using a "beta-advection" method where a weighted average of winds in the upper (200 hPa) and lower (850 hPa) troposphere are used to guide the forward motion of storms. Subsequently, a deep neural network–based approach is used in RAFT to generate intensity along tracks (*40*). Eleven environmental predictors that play a key role in hurricane intensification (*71*, *40*) are estimated from reanalysis and climate models and used with the intensity component of RAFT to produce hurricane intensity along tracks: current intensity, intensity change in the previous 6 hours, vertical wind shear estimated between 200 and 850 hPa, zonal wind at 200 hPa, maximum potential intensity, latitude, longitude, equivalent potential temperature at 1000 hPa, relative humidity averaged between 700- and 850-hPa levels, zonal component of storm motion, and distance to the nearest major landmass. While an overview of RAFT has been documented previously (*40*), see text S1 for a detailed discussion of how RAFT is combined with CMIP6 models to project hurricane activity into the future.

Stationary wave model

To understand the causes behind the projected changes in steering flow, we use a nonlinear SWM (*41*). Using the SWM, we performed a set of numerical sensitivity experiments to explore the mechanisms responsible for the changes in the large-scale winds and hence the steering flow. The SWM takes the basic state (which includes zonal-mean horizontal winds, air temperature, and surface pressure), diabatic heating, transient fluxes, and orography as inputs to generate the quasi–steady-state large-scale dynamical fields. For further details regarding the SWM, its validation, and the various experiments performed, see text S3 and table S1.

Calculations

The CHF is estimated as the number of 6-hour overland hurricane track locations per square degree per year. All storm locations where the intensity exceeds a threshold are considered in this calculation. In the track model of RAFT, we use a 2-day cutoff to truncate tracks over land. Furthermore, at the end of the 2-day period following landfall, storms reach an intensity of about 25 knots on average in observations (*72*). On the basis of the method of quantile mapping (*73*), a 25-knot threshold in observations translates to 21.5 knots when RAFT is used with CMIP6 models. Thus, to ensure consistency between CHF estimates based on the track model, and those based on including the intensity model along with the track model, we use a threshold of 25 knots for RAFT when used with reanalysis and a threshold of 21.5 knots when RAFT is used with CMIP6 models. However, note that our main conclusions are not very sensitive to the threshold and similar results are obtained using a 1-day cutoff.

Changes in steering flow cause changes in CHF primarily through translation speed and landfall, especially in the region close to the coast. To separate the contribution of changes in storm translation speed and landfall to the total CHF change,

Downloaded from https://www.science.org on June 18, 2024

consider the following equation

$$\mathrm{CHF}_{\mathrm{hist}} = n_{\mathrm{hist}} \frac{l}{\text{time step} * v_{\mathrm{hist}}} \quad (1)$$

Here, n is the number of hurricane tracks passing through a grid, l is the grid length, v is the translation speed, and "time step" is 6 hours. The subscript "hist" indicates the historical period. In other words, the equation indicates that the CHF varies directly with the number of storms passing through a region and inversely with the translation speed of storms in that region. Similarly, for the future period, one can write the equation as

$$\mathrm{CHF}_{\mathrm{future}} = n_{\mathrm{future}} \frac{l}{\text{time step} * v_{\mathrm{future}}} \quad (2)$$

To isolate the role of translation, let us assume a scenario with no change in the number of hurricanes passing through a grid. Then, the CHF for the future period ($\mathrm{CHF}_{\mathrm{future}}$) can be expressed as the sum of the CHF for the historical period ($\mathrm{CHF}_{\mathrm{hist}}$) and the effect of translation speed change on CHF ($\mathrm{CHF}_{\mathrm{trans}}$). Now, combining Eqs. 1 and 2, we get

$$\frac{\mathrm{CHF}_{\mathrm{hist}} + \mathrm{CHF}_{\mathrm{trans}}}{\mathrm{CHF}_{\mathrm{hist}}} = \frac{v_{\mathrm{hist}}}{v_{\mathrm{future}}} \quad (3)$$

From this, $\mathrm{CHF}_{\mathrm{trans}}$ can be calculated as

$$\mathrm{CHF}_{\mathrm{trans}} = \mathrm{CHF}_{\mathrm{hist}} \left(\frac{v_{\mathrm{hist}}}{v_{\mathrm{future}}} - 1 \right) \quad (4)$$

Last, the effect of landfall change on CHF ($\mathrm{CHF}_{\mathrm{land}}$) can be estimated as

$$\mathrm{CHF}_{\mathrm{land}} = \mathrm{CHF}_{\mathrm{future}} - \mathrm{CHF}_{\mathrm{hist}} - \mathrm{CHF}_{\mathrm{trans}} \quad (5)$$

Supplementary Materials

This PDF file includes:

Texts S1 to S3
Figs. S1 to S10
Table S1
References

REFERENCES AND NOTES

1. J. Weinkle, C. Landsea, D. Collins, R. Musulin, R. P. Crompton, P. J. Klotzbach, R. Pielke, Normalized hurricane damage in the continental United States 1900–2017. *Nat. Sustain.* **1**, 808–813 (2018).
2. P. J. Klotzbach, S. G. Bowen, R. Pielke, M. Bell, Continental U.S. hurricane landfall frequency and associated damage: Observations and future risks. *Bull. Am. Meteorol. Soc.* **99**, 1359–1376 (2018).
3. A. Grinsted, P. Ditlevsen, J. H. Christensen, Normalized US hurricane damage estimates using area of total destruction, 1900-2018. *Proc. Natl. Acad. Sci. U.S.A.* **116**, 23942–23946 (2019).
4. J. S. Petterson, L. D. Stanley, E. Glazier, J. Philipp, A preliminary assessment of social and economic impacts associated with Hurricane Katrina. *Am. Anthropol.* **108**, 643–670 (2006).
5. J. B. Halverson, T. Rabenhorst, Hurricane Sandy: The science and impacts of a superstorm. *Weatherwise* **66**, 14–23 (2013).
6. J. D. Woodruff, J. L. Irish, S. J. Camargo, Coastal flooding by tropical cyclones and sea-level rise. *Nature* **504**, 44–52 (2013).
7. C. M. Little, R. M. Horton, R. E. Kopp, M. Oppenheimer, G. A. Vecchi, G. Villarini, Joint projections of US East Coast sea level and storm surge. *Nat. Clim. Change* **5**, 1114–1120 (2015).
8. T. Dinan, Projected increases in hurricane damage in the United States: The role of climate change and coastal development. *Ecol. Econ.* **138**, 186–198 (2017).
9. A. Gori, N. Lin, D. Xi, K. Emanuel, Tropical cyclone climatology change greatly exacerbates US extreme rainfall–surge hazard. *Nat. Clim. Change* **12**, 171–178 (2022).
10. T. Knutson, J. C. Suzana, J. C. L. Chan, K. Emanuel, C.-H. Ho, K. James, K. Mohapatra, M. Satoh, M. Sugi, K. Walsh, L. Wu, Tropical cyclones and climate change assessment: Part II: Projected response to anthropogenic warming. *Bull. Am. Meteorol. Soc.* **101**, E303–E322 (2020).
11. K. Emanuel, Response of global tropical cyclone activity to increasing CO_2: Results from downscaling CMIP6 models. *J. Climate* **37**, 57–70 (2020).
12. K. Emanuel, Increasing destructiveness of tropical cyclones over the past 30 years. *Nature* **436**, 686–688 (2005).
13. M. A. Bender, T. R. Knutson, R. E. Tuleya, J. J. Sirutis, G. A. Vecchi, S. T. Garner, I. M. Held, Modeled impact of anthropogenic warming on the frequency of intense atlantic hurricanes. *Science* **327**, 454–458 (2010).
14. A. H. Sobel, S. J. Camargo, T. M. Hall, C.-Y. Lee, M. K. Tippett, A. A. Wing, Human influence on tropical cyclone intensity. *Science* **353**, 242–246 (2016).
15. K. Walsh, S. J. Camargo, T. Knutson, J. Kossin, T.-C. Lee, H. MuraKami, C. Patricola, Tropical cyclones and climate change. *Trop. Cyclone Res. Rev.* **8**, 240–250 (2019).
16. J. P. Kossin, A global slowdown of tropical-cyclone translation speed. *Nature* **558**, 104–107 (2018).
17. J. P. Kossin, Reply to: Moon, I.-J. et al.; Lanzante, J.R. *Nature* **570**, E16–E22 (2019).
18. G. Zhang, H. Murakami, T. R. Knutson, R. Mizuta, K. Yoshida, Tropical cyclone motion in a changing climate. *Sci. Adv.* **6**, eaaz7610 (2020).
19. D. B. Wright, T. R. Knutson, J. A. Smith, Regional climate model projections of rainfall from U.S. landfalling tropical cyclones. *Clim. Dyn.* **45**, 3365–3379 (2015).
20. C. M. Patricola, M. F. Wehner, Anthropogenic influences on major tropical cyclone events. *Nature* **563**, 339–346 (2018).
21. O. Guzman, H. Jiang, Global increase in tropical cyclone rain rate. *Nat. Commun.* **12**, 5344 (2021).
22. S. Wang, R. Toumi, Recent migration of tropical cyclones toward coasts. *Science* **371**, 514–517 (2021).
23. T. M. Hall, J. P. Kossin, Hurricane stalling along the North American coast and implications for rainfall. *npj Clim. Atmos. Sci.* **2**, 17 (2019).
24. K. Balaguru, G. R. Foltz, L. R. Leung, W. Xu, D. Kim, H. Lopez, R. West, Increasing hurricane intensification rate near the US Atlantic coast. *Geophys. Res. Lett.* **49**, e2022GL099793 (2022).
25. M. Ting, J. P. Kossin, S. J. Camargo, C. Li, Past and future hurricane intensity change along the U.S. East coast. *Sci. Rep.* **9**, 7795 (2019).
26. L. Li, P. Chakraborty, Slower decay of landfalling hurricanes in a warming world. *Nature* **587**, 230–234 (2020).
27. S. J. Camargo, A. A. Wing, Increased tropical cyclone risk to coasts. *Science* **371**, 458–459 (2021).
28. G. A. Vecchi, B. J. Soden, Increased tropical atlantic wind shear in model projections of global warming. *Geophys. Res. Lett.* **34**, L08702 (2007).
29. J. P. Kossin, Hurricane intensification along United States coast suppressed during active hurricane periods. *Nature* **541**, 390–393 (2017).
30. J. P. Kossin, S. J. Camargo, M. Sitkowski, Climate modulation of North Atlantic hurricane tracks. *J. Climate* **23**, 3057–3076 (2010).
31. A. J. Colbert, B. J. Soden, G. A. Vecchi, B. P. Kirtman, The impact of anthropogenic climate change on North Atlantic tropical cyclone tracks. *J. Climate* **26**, 4088–4095 (2013).
32. A. J. Garner, R. E. Kopp, B. P. Horton, Evolving tropical cyclone tracks in the North Atlantic in a warming climate. *Earth's Future* **9**, e2021EF002326 (2021).
33. T. M. Hall, J. P. Kossin, T. Thompson, J. McMahon, U.S. tropical cyclone activity in the 2030s based on projected changes in tropical sea surface temperature. *J. Climate* **34**, 1321–1335 (2021).
34. T. R. Knutson, J. J. Sirutis, M. A. Bender, R. E. Tuleya, B. A. Schenkel, Dynamical downscaling projections of late twenty-first-century U.S. landfalling hurricane activity. *Clim. Change* **171**, 28 (2022).
35. K. Emanuel, S. Ravela, E. Vivant, C. Risi, A statistical deterministic approach to hurricane risk assessment. *Bull. Am. Meteorol. Soc.* **87**, 299–314 (2006).
36. C.-Y. Lee, M. K. Tippett, A. H. Sobel, S. J. Camargo, An environmentally forced tropical cyclone hazard model. *J. Adv. Model. Earth Syst.* **10**, 223–241 (2018).
37. J. V. Manganello, K. I. Hodges, J. L. K. III, B. A. Cash, L. Marx, T. Jung, D. Achuthavarier, J. M. Adams, E. L. Altshuler, B. Huang, E. K. Jin, C. Stan, P. Towers, N. Wedi, Tropical cyclone climatology in a 10-km global atmospheric GCM: Toward weather-resolving climate modeling. *J. Climate* **25**, 3867–3893 (2012).
38. S. J. Camargo, A. A. Wing, Tropical cyclones in climate models. *WIREs Clim. Change* **7**, 211–237 (2016).

Downloaded from https://www.science.org on June 18, 2024

39. N. Bloemendaal, I. D. Haigh, H. de Moel, S. Muis, R. J. Haarsma, J. C. J. H. Aerts, Generation of a global synthetic tropical cyclone hazard dataset using STORM. *Sci. Data* **7**, 40 (2020).
40. W. Xu, K. Balaguru, A. August, N. Lalo, N. Hodas, M. DeMaria, D. Judi, Deep learning experiments for tropical cyclone intensity forecasts. *Weather Forecast.* **36**, 1453–1470 (2021).
41. M. Ting, L. Yu, Steady response to tropical heating in wavy linear and nonlinear baroclinic models. *J. Atmos. Sci.* **55**, 3565–3582 (1998).
42. H. Murakami, T. L. Delworth, W. F. Cooke, M. Zhao, B. Xiang, P.-C. Hsu, Detected climatic change in global distribution of tropical cyclones. *Proc. Natl. Acad. Sci. U.S.A.* **117**, 10706–10714 (2020).
43. E. Kalnay, M. Kanamitsu, R. Kistler, W. Collins, D. Deaven, L. Gandin, M. Iredell, S. Saha, G. White, J. Woollen, Y. Zhu, A. Leetmaa, R. Reynolds, M. Chelliah, W. Ebisuzaki, W. Higgins, J. Janowiak, K. C. Mo, C. Ropelewski, J. Wang, R. Jenne, D. Joseph, The NCEP/NCAR 40-year reanalysis project. *Bull. Am. Meteorol. Soc.* **77**, 437–471 (1996).
44. H. Hersbach, B. Bell, P. Berrisford, S. Hirahara, A. Horányi, J. Muñoz-Sabater, J. Nicolas, C. Peubey, R. Radu, D. Schepers, A. Simmons, C. Soci, S. Abdalla, X. Abellan, G. Balsamo, P. Bechtold, G. Biavati, J. Bidlot, M. Bonavita, G. Chiara, P. Dahlgren, D. Dee, M. Diamantakis, R. Dragani, J. Flemming, R. Forbes, M. Fuentes, A. Geer, L. Haimberger, S. Healy, R. J. Hogan, E. Hólm, M. Janisková, S. Keeley, P. Laloyaux, P. Lopez, C. Lupu, G. Radnoti, P. Rosnay, I. Rozum, F. Vamborg, S. Villaume, J.-N. Thépaut, The ERA5 global reanalysis. *Q. J. Roy. Meteorol. Soc.* **146**, 1999–2049 (2020).
45. V. Eyring, S. Bony, G. A. Meehl, C. A. Senior, B. Stevens, R. J. Stouffer, K. E. Taylor, Overview of the Coupled Model Intercomparison Project phase 6 (CMIP6) experimental design and organization. *Geosci. Model Dev.* **9**, 1937–1958 (2016).
46. B. C. O'Neill, C. Tebaldi, D. P. Van Vuuren, V. Eyring, P. Friedlingstein, G. Hurtt, R. Knutti, E. Kriegler, J.-F. Lamarque, J. Lowe, G. A. Meehl, R. Moss, K. Riahi, B. M. Sanderson, The scenario model intercomparison project (scenarioMIP) for CMIP6. *Geosci. Model Dev.* **9**, 3461–3482 (2016).
47. B. Wang, B. Xiang, J.-Y. Lee, Subtropical high predictability establishes a promising way for monsoon and tropical storm predictions. *Proc. Natl. Acad. Sci. U.S.A.* **110**, 2718–2722 (2013).
48. A. J. Simmons, The forcing of stationary wave motion by tropical diabatic heating. *Q. J. Roy. Meteorol. Soc.* **108**, 503–534 (1982).
49. B. J. Hoskins, D. J. Karoly, The steady linear response of a spherical atmosphere to thermal and orographic forcing. *J. Atmos. Sci.* **38**, 1179–1196 (1981).
50. S. Manabe, T. B. Terpstra, The effects of mountains on the general circulation of the atmosphere as identified by numerical experiments. *J. Atmos. Sci.* **31**, 3–42 (1974).
51. I. M. Held, M. Ting, H. Wang, Northern winter stationary waves: Theory and modeling. *J. Climate* **15**, 2125–2144 (2002).
52. W. Li, L. Li, M. Ting, Y. Liu, Intensification of northern hemisphere subtropical highs in a warming climate. *Nat. Geosci.* **5**, 830–834 (2012).
53. F. Song, L. R. Leung, J. Lu, L. Dong, Future changes in seasonality of the North Pacific and North Atlantic subtropical highs. *Geophys. Res. Lett.* **45**, 11959–11968 (2018).
54. Y. Wu, R. Seager, M. Ting, N. Naik, T. A. Shaw, Atmospheric circulation response to an instantaneous doubling of carbon dioxide. Part I: Model experiments and transient thermal response in the troposphere. *J. Clim.* **25**, 2862–2879 (2012).
55. E. A. Barnes, L. Polvani, Response of the midlatitude jets, and of their variability, to increased greenhouse gases in the CMIP5 models. *J. Climate* **26**, 7117–7135 (2013).
56. S.-K. Lee, D. B. Enfield, C. Wang, Future impact of differential interbasin ocean warming on Atlantic hurricanes. *J. Climate* **24**, 1264–1275 (2011).
57. A. E. Gill, Some simple solutions for heat-induced tropical circulation. *Q. J. Roy. Meteorol. Soc.* **106**, 447–462 (1980).
58. S.-P. Xie, C. Deser, G. A. Vecchi, J. Ma, H. Teng, A. T. Wittenberg, Global warming pattern formation: Sea surface temperature and rainfall. *J. Climate* **23**, 966–986 (2010).
59. R. Chadwick, P. Good, T. Andrews, G. Martin, Surface warming patterns drive tropical rainfall pattern responses to CO_2 forcing on all timescales. *Geophys. Res. Lett.* **41**, 610–615 (2014).
60. C. Kent, R. Chadwick, D. P. Rowell, Understanding uncertainties in future projections of seasonal tropical precipitation. *J. Climate* **28**, 4390–4413 (2015).
61. A. H. Sobel, J. Nilsson, L. M. Polvani, The weak temperature gradient approximation and balanced tropical moisture waves. *J. Atmos. Sci.* **58**, 3650–3665 (2001).
62. C. S. Bretherton, A. H. Sobel, A simple model of a convectively coupled walker circulation using the weak temperature gradient approximation. *J. Climate* **15**, 2907–2920 (2002).
63. D. J. Raymond, Regulation of moist convection over the west Pacific warm pool. *J Atmos. Sci.* **52**, 3945–3959 (1995).
64. L. Dong, L. R. Leung, F. Song, J. Lu, Uncertainty in El Niño-like warming and California precipitation changes linked by the interdecadal Pacific oscillation. *Nat. Commun.* **12**, 6484 (2021).
65. R. Seager, M. Cane, N. Henderson, D.-E. Lee, R. Abernathey, H. Zhang, Strengthening tropical Pacific zonal sea surface temperature gradient consistent with rising greenhouse gases. *Nat. Clim. Change* **9**, 517–522 (2019).
66. J. Ying, P. Huang, The large-scale ocean dynamical effect on uncertainty in the tropical Pacific SST warming pattern in CMIP5 models. *J. Climate* **29**, 8051–8065 (2016).
67. J. Ying, P. Huang, Cloud–radiation feedback as a leading source of uncertainty in the tropical Pacific SST warming pattern in CMIP5 models. *J. Climate* **29**, 3867–3881 (2016).
68. J. Ma, S.-P. Xie, Regional patterns of sea surface temperature change: A source of uncertainty in future projections of precipitation and atmospheric circulation. *J. Climate* **26**, 2482–2501 (2013).
69. M. Roberts, CMIP6 HighResMIP: Tropical storm tracks as calculated by the TempestExtremes algorithm (Centre for Environmental Data Analysis, 2019).
70. R. J. Haarsma, M. J. Roberts, P. L. Vidale, C. A. Senior, A. Bellucci, Q. Bao, P. Chang, S. Corti, N. S. Fučkar, V. Guemas, J. von Hardenberg, W. Hazeleger, C. Kodama, T. Koenigk, L. R. Leung, J. Lu, J.-J. Luo, J. Mao, M. S. Mizielinski, R. Mizuta, P. Nobre, M. Satoh, E. Scoccimarro, T. Semmler, J. Small, J.-S. von Storch, High resolution model intercomparison project (HighResMIP v1.0) for CMIP6. *Geosci. Model Dev.* **9**, 4185–4208 (2016).
71. M. DeMaria, M. Mainelli, L. K. Shay, J. A. Knaff, J. Kaplan, Further improvements to the statistical hurricane intensity prediction scheme (ships). *Weather Forecast.* **20**, 531–543 (2005).
72. J. Kaplan, M. DeMaria, A simple empirical model for predicting the decay of tropical cyclone winds after landfall. *J. Appl. Meteorol. Climatol.* **34**, 2499–2512 (1995).
73. A. J. Cannon, S. R. Sobie, T. Q. Murdock, Bias correction of GCM precipitation by quantile mapping: How well do methods preserve changes in quantiles and extremes? *J. Climate* **28**, 6938–6959 (2015).
74. A. H. Sobel, A. A. Wing, S. J. Camargo, C. M. Patricola, G. A. Vecchi, C.-Y. Lee, M. K. Tippett, Tropical cyclone frequency. *Earth's Future* **9**, e2021EF002275 (2021).
75. H. Murakami, B. Wang, Patterns and frequency of projected future tropical cyclone genesis are governed by dynamic effects. *Commun. Earth Environ.* **3**, 77 (2022).
76. L. Wu, B. Wang, Assessing impacts of global warming on tropical cyclone tracks. *J. Climate* **17**, 1686–1698 (2004).
77. P. Kelly, L. R. Leung, K. Balaguru, W. Xu, B. Mapes, B. Soden, Shape of Atlantic tropical cyclone tracks and the Indian monsoon. *Geophys. Res. Lett.* **45**, 10–746 (2018).
78. P. A. Ullrich, C. M. Zarzycki, E. E. McClenny, M. C. Pinheiro, A. M. Stansfield, K. A. Reed, TempestExtremes v2.1: A community framework for feature detection, tracking, and analysis in large datasets. *Geosci. Model Dev.* **14**, 5023–5048 (2021).
79. T. R. Knutson, J. J. Sirutis, S. T. Garner, G. A. Vecchi, I. M. Held, Simulated reduction in Atlantic hurricane frequency under twenty-first-century warming conditions. *Nat. Geosci.* **1**, 359–364 (2008).
80. K. Yoshida, M. Sugi, R. Mizuta, H. Murakami, M. Ishii, Future changes in tropical cyclone activity in high-resolution large-ensemble simulations. *Geophys. Res. Lett.* **44**, 9910–9917 (2017).
81. A. S. Daloz, S. J. Camargo, Is the poleward migration of tropical cyclone maximum intensity associated with a poleward migration of tropical cyclone genesis? *Climate Dynam.* **50**, 705–715 (2018).
82. M. F. Wehner, K. A. Reed, B. Loring, D. Stone, H. Krishnan, Changes in tropical cyclones under stabilized 1.5 and 2.0°C global warming scenarios as simulated by the Community Atmospheric Model under the HAPPI protocols. *Earth Syst. Dyn.* **9**, 187–195 (2018).
83. G. Zhang, L. G. Silvers, M. Zhao, T. R. Knutson, Idealized aquaplanet simulations of tropical cyclone activity: Significance of temperature gradients, Hadley circulation, and zonal asymmetry. *J. Atmos. Sci.* **78**, 877–902 (2021).
84. J. Studholme, A. V. Fedorov, S. K. Gulev, K. Emanuel, K. Hodges, Poleward expansion of tropical cyclone latitudes in warming climates. *Nat. Geosci.* **15**, 14–28 (2022).
85. K. Emanuel, Response of global tropical cyclone activity to increasing CO_2: Results from downscaling CMIP6 models. *J. Climate* **34**, 57–70 (2021).
86. I. R. Simpson, R. Seager, M. Ting, T. A. Shaw, Causes of change in Northern Hemisphere winter meridional winds and regional hydroclimate. *Nat. Clim. Change* **6**, 65–70 (2016).
87. B. Hoskins, On the existence and strength of the summer subtropical anticyclones: Bernhard Haurwitz memorial lecture. *Bull. Am. Meteorol. Soc.* **77**, 1287–1292 (1996).
88. S. Nigam, C. Chung, E. DeWeaver, ENSO diabatic heating in ECMWF and NCEP–NCAR reanalyses, and NCAR CCM3 simulation. *J. Climate* **13**, 3152–3171 (2000).
89. A. Cherchi, H. Annamalai, S. Masina, A. Navarra, South Asian summer monsoon and the Eastern Mediterranean climate: The monsoon-desert mechanism in CMIP5 simulations. *J. Climate* **27**, 6877–6903 (2014).

Acknowledgments: We acknowledge the World Climate Research Program's Working Group on Coupled Modeling, which is responsible for CMIP5 and CMIP6, and thank the climate modeling groups for producing and making available the model output. **Funding:** This research was supported by the U.S. Department of Energy (DOE) Office of Science Biological

Downloaded from https://www.science.org on June 18, 2024

and Environmental Research as part of the Regional and Global Model Analysis (RGMA) program area through the Water Cycle and Climate Extremes Modeling (WACCEM) project and as part of the RGMA and MultiSector Dynamics (MSD) program areas through the collaborative, multiprogram Integrated Coastal Modeling (ICoM) project. The research used computational resources from the National Energy Research Scientific Computing Center (NERSC), a U.S. DOE User Facility supported by the Office of Science under contract DE-AC02-05CH11231. The Pacific Northwest National Laboratory is operated for U.S. DOE by Battelle Memorial Institute under contract DE-AC05-76RL01830. For CMIP5 and CMIP6, the U.S. DOE's Program for Climate Model Diagnostics and Intercomparison provides coordinating support and led the development of software infrastructure in partnership with the Global Organization for Earth System Science Portals. **Author contributions:** K.B. developed the main idea and methodology with inputs from W.X., C.-C.C., L.R.L., D.R.J., and S.M.H. W.X. performed simulations with RAFT. C.-C.C. conducted the SWM experiments. K.B., C.-C.C., W.X., and L.R.L. wrote the paper and performed analysis. D.R.J., S.M.H., M.F.W., J.P.K., and M.T. provided feedback and helped in the preparation of the manuscript. **Competing interests:** The authors declare that they have no competing interests. **Data and materials availability:** All data needed to evaluate the conclusions in the paper are present in the paper and/or the Supplementary Materials. Hurricane track data from RAFT analyzed and presented in this study are available at https://zenodo.org/record/7465149#.Y6JQJ-zMJeV. SWM simulations used in this study are available at https://zenodo.org/record/7459326#.Y6DhAuzMJeV%7D. The sources for other publicly available data used in this study are as follows: Best track data (www.nhc.noaa.gov/data/#hurdat), ERA5 reanalysis data (www.ecmwf.int/en/forecasts/datasets/reanalysis-datasets/era5), NCEP/NCAR reanalysis data (https://psl.noaa.gov/data/gridded/data.ncep.reanalysis.html), CMIP6 data for the historical and future periods (https://esgf-node.llnl.gov/projects/cmip6/), and HighResMIP hurricane track data (https://catalogue.ceda.ac.uk/uuid/438268b75fed4f27988dc02f8a1d756d).

Submitted 23 September 2022
Accepted 6 March 2023
Published 7 April 2023
10.1126/sciadv.adf0259

Downloaded from https://www.science.org on June 18, 2024